33rd Annual International Conference of the IEEE EMBS
Boston, Massachusetts USA, August 30 - September 3, 2011

Automatic Optic Disc Segmentation with Peripapillary Atrophy Elimination

Jun Cheng, Jiang Liu, Damon Wing Kee Wong, Fengshou Yin,
Carol Cheung, Mani Baskaran, Tin Aung, and Tien Yin Wong

***Abstract*— Optic disc segmentation from retinal fundus image is a fundamental but important step for automatic glaucoma diagnosis. In this paper, an optic disc segmentation method is proposed based on peripapillary atrophy elimination. The elimination is done through edge filtering, constraint elliptical Hough transform and peripapillary atrophy detection. With the elimination, edges that are likely from non-disc structures especially peripapillary atrophy are excluded to make the segmentation more accurate. The proposed method has been tested in a database of 650 images with disc boundaries marked by trained professionals manually. The experimental results by the proposed method show average m_1, m_2 and m_{VD} of 10.0%, 7.4% and 4.9% respectively. It can be used to compute cup to disc ratio as well as other features for application in automatic glaucoma diagnosis systems.**

I. Introduction

In the past years, localization of the optic disc (OD) from retinal fundus images has been investigated extensively [1][2]. The main task of these algorithms is to find the location of OD so that it wound not be confounded with large exudative lesions. For some applications such as automatic glaucoma diagnosis from retinal fundus images, automatic segmentation of OD is needed. The objective of OD segmentation is to find its boundary. Fig. 1 shows two examples, where the lines in green are the ground truth OD boundaries to be determined. There are several reasons to get OD boundary precisely for glaucoma diagnosis application. Firstly, vertical disc diameter is the denominator to compute the vertical cup to disc ratio (CDR) [3], which is a critical factor used by many ophthalmologists for the diagnosis; secondly, the size of OD itself is a factor in the diagnosis [4]; thirdly, it is necessary to have the OD boundary to determine compliance of ISNT and optic rim thinning [5]. Thus, automatic OD segmentation is a fundamental but very important step for the diagnosis.

Several approaches have been proposed for OD segmentation. Deformable model is used in [6][7]. However, it is sensitive to poor initialization. In [8], level set is used. The approach is often affected by a large number of blood vessels entering the disc as well as peripapillary atrophy (PPA) that slows down the evolution of the level set to reach the disc boundary. In [9], circular Hough transform is used. Hough transform using all edge pixels detected by traditional edge detection algorithms such as 'Sobel' [10] or 'Canny' [11] often produces un-desired results. One common limitation of these algorithms is that the presence of PPA has not been considered and the resultant segmentation often mistakes PPA as part of OD. For example, the lines in blue are often detected as OD boundaries in Fig. 1 with PPA being included. Such a result often leads to an under-estimated CDR and/or inaccurate ISNT compliance. Since PPA appears often among glaucoma patients, excluding PPA area from OD, i.e., PPA elimination, is necessary to measure OD diameters for clinical use [12]. To the best of our knowledge, existing automatic OD segmentation algorithms did not consider PPA. Besides PPA, blood vessels and even some of optic cups may affect the OD segmentation sometimes and are considered as well in this paper. The paper is organized as follows. In Section I, we have given an introduction of the background and motivation for the method. In Section II, we introduce the methods in details. Section III shows the experimental results, followed by the conclusions in the last section.

This work was supported in part by the Agency for Science, Technology and Research, Singapore, under SERC grant 092-148-00731.

J. Cheng, J. Liu, D. W. K. Wong, and F. Yin are with Institute for Infocomm Research, A*Star, Singapore. C. Cheung and M. Baskaran are with Singapore Eye Research Institute. T. Aung and T. Y. Wong are with Singapore Eye Research Institute and National University of Singapore.

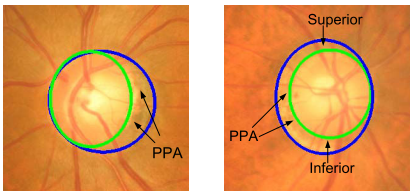

(a) (b)

Fig. 1. Green: ground truth OD boundary, Blue: detected OD boundary

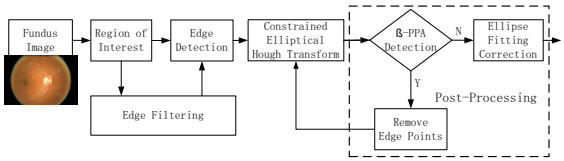

Fig. 2. Flow Chart of the Method

II. Methodology

In this paper, OD is approximated as ellipse as in [8]. The flow chart of the segmentation is summarized in Fig. 2. The PPA elimination is conducted in three parts: an edge filtering, a constraint elliptical Hough transform, and a β-PPA detection.

A. Region of Interest and Edge Detection

Region of interest (ROI) extraction is similar to OD localization. It can be done by localization algorithms as in [1][2],

however the fringe removal based method in [13] is used to get the ROI image I in this paper because of its simplicity. Arbitrarily including all edges from I is unnecessary. We propose to extract edges as follows. First, a low pass filter is applied on the image to smooth away noise. In this paper, a 2D mean filter is used to get the smoothed image $\tilde{I}$. Then for each row profile L from $\tilde{I}$, compute its first derivative L'. The local maximums and minimums of L' are the possible horizontal edges from OD boundary in this row. Inspired by the observation that the pixel values increase when entering the disc and decrease when exiting, only local maximums from the left half of each row and local minimums from right half are used. Similarly, local maximums and minimums from column profiles are obtained to get vertical edges as well to form candidate disc boundaries.

B. Edge filtering

The first PPA elimination is through edge filtering (EF). There are two types of PPA: α and β. α-PPA represents pigmentary and structural irregularity of retinal pigment epithelial (RPE) cells. β-PPA represents a complete loss of the RPE cells. α-PPA is normally darker than OD while the OD is the brightest part within the ROI. Excluding edges from α-PPA can be done by comparing the ROI with a threshold T_D followed by a morphological closing processing, i.e., $E = imdilate(D)$, where $imdilate(\cdot)$ denotes a morphological dilation, D is a binary matrix computed by:

$$D(x,y) = \begin{cases} 1 & I(x,y) > T_D \\ 0 & \texttt{otherwise} \end{cases} \quad (1)$$

In this paper, T_D is initialized to be the mean intensity in the ROI and increased until the number of pixels brighter than T_D is no larger than 20% of total number of pixels. The value 20% is empirically determined based on typical OD size. A candidate edge (x, y) with $E(x, y) = 0$ would be excluded. The dilation is necessary to preserving OD boundary pixels which often have relatively lower pixel intensity. Excluding edges from β-PPA is much more difficult as it has a color similar to OD. In this paper, we propose to apply β-PPA detection followed by edge removal later.

Besides PPA, blood vessels might affect the segmentation as well. Across the blood vessels, the pixel intensity decreases first before increasing again shortly. Thus, the blood vessel corresponds to one local minimum followed by one local maximum in the same row/column. In this paper, we exclude every pair where a local minimum is followed by a local maximum in its nearby within the same row/column. In some occasional case, optic cup with distinctive boundary affect the OD segmentation as well. However, in such a scenario, the brightest part is close to 255. Thus, edges close to pixels with highest intensity are excluded.

C. Constrained Elliptical Hough Transform

OD is approximately an ellipse with parametric representation given by:

$$\begin{aligned} x(t) &= x_c + a\cos t\cos\phi - b\sin t\sin\phi \\ y(t) &= y_c + a\cos t\sin\phi + b\sin t\cos\phi \end{aligned}, \quad (2)$$

where $t \in [0, 2\pi]$, (x_c, y_c) is row and column coordinate of the center, a and b are the vertical and horizontal radius respectively, and ϕ is the rotation angle of the ellipse. OD has a slightly oval shape with vertical diameter being about 7%-10% larger than horizontal one [14]. Because of crescent shape [15] of PPA (both α and β type) appears on nasal and/or temporal side of OD, PPA together with OD often form an ellipse wider in horizontal as in Fig. 1(a). Thus, the second PPA elimination is done by a constrained elliptical Hough transform (CEHT) summarized as follows:

1) Set parameter (a, b, ϕ) for ellipse.
2) For each edge point (x_e, y_e), draw an ellipse centered at (x_e, y_e) with (a, b, ϕ) and increment all coordinates that the perimeter of the ellipse passes through in the accumulator A corresponding to the parameters.
3) Update (a, b, ϕ) and repeat step 2 for all (a, b, ϕ) from the parameter space.
4) Find the maximum value in A to get an ellipse centered at (x_1, y_1) and corresponding parameters (a_1, b_1, ϕ_1).
5) If $b_1/a_1 > \gamma$, then find the maximum value in A subject to $b/a \leq \gamma$ to get a second ellipse centered at (x_2, y_2).
6) Determine the OD boundary as the second ellipse if $A(x_2, y_2)/A(x_1, y_1) > T_A$, otherwise, the first one.

The idea is that if $b_1/a_1 > \gamma$, there is a higher chance that the first detected ellipse include some of PPA. Thus we would further check if there is another slightly weaker ellipse with $b/a \leq \gamma$. If so, the second one is more likely to be the disc boundary with reduced chance to mistake PPA as part of OD.

D. β-PPA Detection

Although the CEHT helps avoid some PPAs via embedding prior knowledge of the OD shape in the detection, it does not work if $b_1/a_1 \leq \gamma$. Such a case happens often when β-PPA with moderate size or larger appears on inferior and/or superior as in Fig. 1(b) without making $b_1/a_1 > \gamma$. Thus, the third PPA elimination is implemented by β-PPA detection. Since the PPA affects the segmentation by being mistaken as part of OD, a ring area, as shown in Fig. 3, is empirically determined from the detected disc boundary (line in blue) for further analysis. Inspired by the texture within β-PPA compared with OD, we extract all local maximums and minimums from smoothed row and column profiles within the ring, similar to that in Section II-A. To be distinguishable from the edge points in Section II-A, they are named as feature points. In each quadrant Q_i, the numbers of feature points from rows and columns are counted separately. When the numbers of feature points exceed a certain level in the quadrant, β-PPA is considered as present in Q_i. The threshold level used is learned by comparing the cases with β-PPA vs. the cases without. Then the edge points along the detected disc boundary from Q_i are removed. The CEHT would be re-applied to get a new disc boundary.

E. Ellipse Fitting Correction

In some cases, the ellipse fitting over-fits the OD with the resultant ellipse boundary lying away from the true boundary in some segment as shown in Fig. 4. To improve the segmentation, we search on two sides of the current detected disc

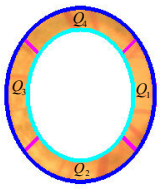

Fig. 3. ROI ring for β-PPA analysis

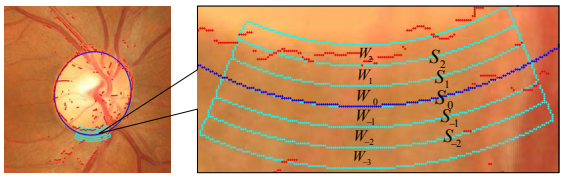

Fig. 4. Ellipse Correction: edge points in red and corresponding disc boundary in blue

boundary in quadrant Q_i, $i = 1, 2, 3, 4$. The search region is from each quadrant and divided into several overlapping windows, as illustrated in Fig. 4 for Q_2. When the number of edge points in S_0 is below certain level, we search in the region nearby for the nearest window $S_j = W_j \cup W_{j-1}, j = -2, ..., 2$, with more edge points. If such a new window is found, adjust the ellipse parameters such that the new disc boundary passing through the new window.

III. Experimental Results

A. *ORIGA ^{light} Database and Evaluation Metrics*

The ORIGA ^{light} [16] database which contains 650 images is used in this paper. PPA appears in more than 200 images. The OD boundaries have been manually marked by trained professionals. Several metrics are commonly used to evaluate segmentation accuracy: overlapping error $m_1 = (1 - \frac{OD_{seg} \cap OD_{ref}}{OD_{seg} \cup OD_{ref}})$, relative absolute area diffeence $m_2 = \frac{|OD_{seg} - OD_{ref}|}{OD_{ref}}$, where OD_{seg} and OD_{ref} denote the segmented and the ground truth disc respectively. In addition, accuracy of vertical disc diameter, the denominator to compute CDR, is computed as: $m_{VD} = \frac{|VD_{seg} - VD_{ref}|}{VD_{ref}}$, where VD_{seg} and VD_{ref} represent the vertical diameter of the segmented disc and corresponding ground truth respectively. A lower score indicates a better performance with 0 indicates perfect segmentation in these metrics.

B. *Results*

We first show several examples of the segmentation results together with ground truth to highlight the benefit of EF. In Fig. 5, the red and blue lines are the results with and without EF and the green lines are the ground truth. For images without PPA such as Fig. 5(a), both results are close to the ground truth. For images with PPA as shown in Fig. 5(b)-Fig. 5(g), the method without EF is often trapped by the PPA boundary while the proposed method finds the disc boundary more accurately. Fig. 5(h) is an example where both methods fail to find the disc boundary accurately due to low contrast disc boundary. In CEHT, γ is set to be 0.95, slightly larger than typical ratio of horizontal diameter to vertical diameter. T_A is set to be 0.9, slightly lower than the ratio of the perimeter of the ground truth OD to that of the strongest ellipse from images with mild PPA. Fig. 6 shows some images for comparison of the results with and without the post-processing. The first row shows the benefit with β-PPA detection. The lines in magenta and cyan are the results with and without β-PPA detection. The second row shows the benefit from ellipse fitting correction. The red lines show the final results. From the comparison, we can see post-processing improve the results.

Method	m_1	m_2	m_{VD}
Sobel+CHT	26.1%±24.5%	22.8%±33.1%	11.2%±12.0%
Sobel+EHT	25.2%±24.3%	17.7%±20.9%	8.7%±9.3%
Level Set	23.1%±23.4%	29.9%± 49.1%	15.6%±23.0%
Before PPA detection	13.0%±9.2%	11.9%±13.1%	6.0%±6.1%
Proposed	10.0%±8.5%	7.4%±10.6%	4.9%±5.9%

TABLE I

Mean ± standard deviation of the metrics from 650 images by various segmentation methods

A quantitative comparison with three other methods is also given. The first method uses Sobel edge detection combined with circular Hough transform as in [9]. In the second method, circular Hough transform is replaced with elliptical Hough transform. The third is the level-set approach [8]. Besides the above methods, we also show the results before β-PPA detection. Table I shows the means and standard deviations of the evaluation metrics m_1, m_2, and m_{VD} based on the performance of the 650 images. Fig. 7 shows the metric values for each image by various methods, sorted from least to most. From the comparison, it can be concluded that the proposed method outperform the other three methods.

IV. Conclusions

Automatic OD segmentation is a fundamental but necessary step for developing automatic glaucoma diagnosis systems. In this paper, we propose a method for automatic OD segmentation. Different from previous methods, PPA has been considered through EF, CEHT, and β-PPA detection in the post-processing for the first time. With the PPA elimination, the proposed method outperforms three other methods with a great reduction of average overlapping errors. It is beneficial to compute CDR as well as other features more accurately and thus important for automatic glaucoma diagnosis. However, it still replies on a good segmentation of optic cup to evaluate quantitatively how the disc segmentation improves the automatic glaucoma diagnosis, which would be our future work.

References

[1] A. Hoover and M. Goldbaum, "Locating the optic nerve in a retinal image using the fuzzy convergence of the blood vessels," *IEEE Trans. on Medical Imaging*, vol. 22, pp. 951–958, 2003.

[2] M. Foracchia, E. Grisan, and A. Ruggeri, "Detection of optic disc in retinal images by means of a geometrical model of vessel structure," *IEEE Trans. on Medical Imaging*, vol. 23, no. 10, pp. 1189–1195, 2004.

[3] Damms T. and Dannheim F., "Sensitivity and specificity of optic disc parameters in chronic glaucoma," *Invest. Ophth. Vis. Sci.*, vol. 34, pp. 2246–2250, 1993.

[4] Michael D. and Hancox O.D., "Optic disc size, an important consideration in the glaucoma evaluation," *Clinical Eye and Vision Care*, vol. 11, pp. 59–62, 1999.

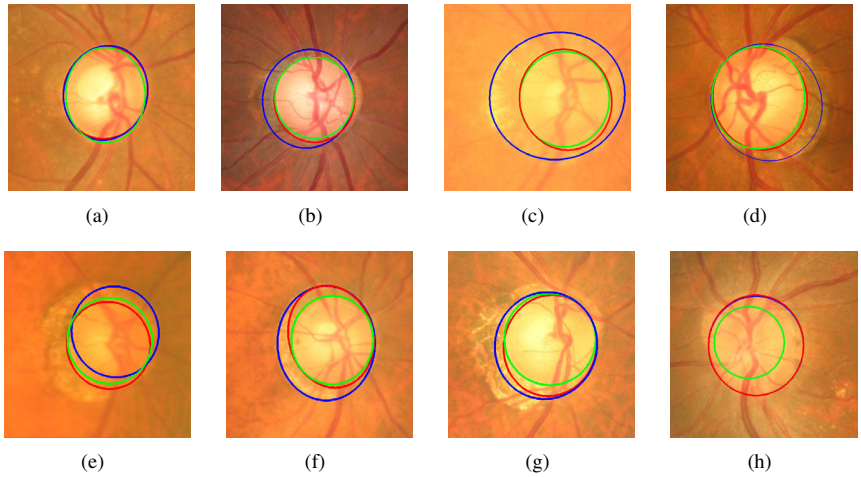

Fig. 5. Sample results (Blue: without EF, Red: with EF, Green: ground truth)

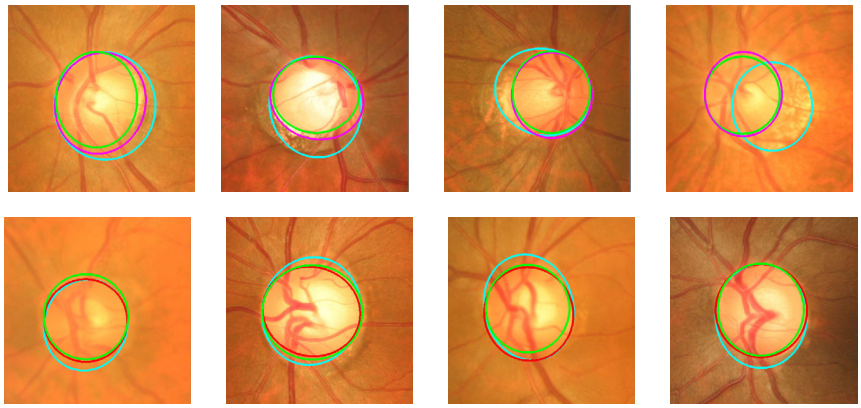

Fig. 6. Sample results (Cyan: before β-PPA detection, Magenta: after β-PPA detection, Red: with ellipse correction, Green: ground truth)

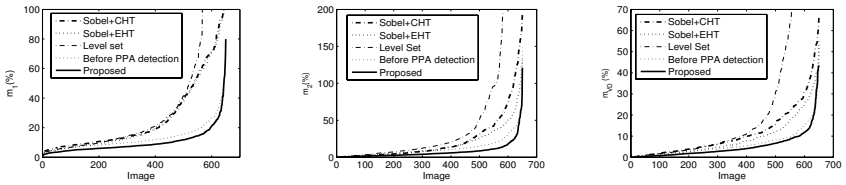

Fig. 7. m_1, m_2, and m_{VD} for 650 images by different methods sorted from minimum to maximum. A lower score indicates a better performance.

[5] N. Harizman, C. Oliveira, A. Chiang, C. Tello, M. Marmor, R. Ritch, and JM. Liebmann, "The isnt rule and differentiation of normal from glaucomatous eyes," vol. 124, pp. 1579–1583, 2006.

[6] H. Li and O. Chutatape, "Boundary detection of optic disc by a modified asm method," *Pattern Recognition*, vol. 36, pp. 2093–2104, 2003.

[7] J. Xu, O. Chutatape, E. Sung, C. Zheng, and P.C.T. Kuan, "Optic disk feature extraction via modified deformable model technique for glaucoma analysis," *Pattern Recognition*, vol. 40, pp. 2063–2076, 2007.

[8] Z. Zhang, J. Liu, N. S. Cherian, Y. Sun, J. H. Lim, W.K.Wong, N. M. Tan, S. Lu, H. Li, and T. Y. Wong, "Convex hull based neuro-retinal optic cup ellipse optimization in glaucoma diagnosis," *Int. Conf. of IEEE Eng. in Med. and Bio. Soc.*, pp. 1441–1444, 2009.

[9] X. Zhu and R. M. Rangayyan, "Detection of the optic disc in images of the retina using the hough transform," pp. 3546–3549, 2008.

[10] Gonzalez RC and Woods RE, "Digital image processing," 2002.

[11] J. Canny, "A computational approach to edge detection," *IEEE Trans. Pattern Analysis and Machine Intelligence*, vol. 8, pp. 679–698, 1986.

[12] N. Amerasinghe, T. Y. Wong, W. L. Wong, S. Y. Shen, S. C. Loon, S. M. Saw, P. J. Foster, and T. Aung, "Determinants of the optic cup to disc ratio in an asian populations: the singapore malay eye study," *Arch Ophthalmo.*, 2008.

[13] Z. Zhang, B.H. Lee, J. Liu, D.W.K. Wong, N.M. TAN, J.H. Lim, F.S. Yin, W.M. Huang, and H. Li, "Optic disc region of interest localization in fundus image for glaucoma detection in argali," *Proc. of Int. Conf. on Industrial Electronics & Applications*, pp. 1686–1689, 2010.

[14] J. B. Jonas, W. M. Budde, and S. Panda-Jonas, "Ophthalmoscopic evaulation of the optic nerve head," *Surv. Ophthalmol.*, pp. 293–320, 1999.

[15] J. A. Giaconi, S. K. Law, A. L. Coleman, and J. Caprioli, *Pearls of Glaucoma Management*, Springer Heidelberg Dordrecht London New York, 2010.

[16] Z. Zhang, F. Yin, J. Liu, W. K. Wong, N. M. Tan, B. H. Lee, J. Cheng, and T. Y. Wong, "Origa-light: An online retinal fundus image database for glaucoma analysis and research," *Int. Conf. of IEEE Eng. in Med. and Bio. Soc.*, pp. 3065–3068, 2010.